4^{th} URSI AT-RASC, Gran Canaria, 19 – 24 May 2024

Impact of Antenna Load on Embedded Element Patterns in Aperture Arrays: the Single Fault Case

Georgios Kyriakou*(1), Maria Kovaleva(2) and David B. Davidson(2)
(1) INAF-Arcetri Astrophysical Observatory, Largo Enrico Fermi 5, 50125, Florence, Italy, georgios.kyriakou@inaf.it
(2) International Centre for Radio Astronomy Research (ICRAR-Curtin), 1 Turner Avenue, Bentley, WA 6102, Australia

Abstract

We present a simplified equation of the transformation between Embedded Element Patterns (EEPs) of an array of identically loaded elements, with the exception of one faulty termination of arbitrary offset. This new expression is proven to need only one column of the loaded admittance matrix to work out the new EEPs from the identically loaded ones. It can also be depicted as a circuit equivalent by superimposing two contributions of the EEPs referred to the original, scaled unitary matrix load for all elements, one of which multiplied by a proper voltage transfer function. Applications of this representation are also discussed. Finally, simple dipole simulations, as well as more complex EEPs of a real as-deployed radio astronomical antenna array corroborate the formula both by forward (EEPs) as well as inverse (impedance fault) calculations.

1 Introduction

Characterisation of antenna arrays for radio astronomy in terms of Embedded Element Patterns (EEPs) under different loading conditions and their subsequent application to beam steering is a well-developed theory [1]. Inverse problems, such as finding the loading condition that leads to specific, usually measured EEPs are also of interest. This is an important case for fault diagnosis, as the front-end on which a phased array is mounted can vary because of the failure of low-noise amplifiers (LNAs). This can happen due to environmental effects that are not uncommon in operation fields, and leads to electrical and mechanical damage or other technical problems. As has already been shown in [2], in the case of failing LNAs, matrix transformations can be used to compute the resulting EEPs and assess the errors in an array pattern caused by malfunctioning LNAs. These transformations can be easily inverted to obtain the loading condition of an array, but since the loads apply only on the diagonal elements of a mutual impedance matrix (N ports), there is redundancy in the inverted relationships that calculate N non-zero elements using $N \times M$ matrices, where M is the number of simulation or measurement points in the 3D far-field patterns.

To tackle this issue, a perturbative linear algebra derivation has proven useful in computing the new EEPs under faulty termination. Recently, Buck et. al. [3] showed that a more complicated relationship arises when each EEP has to be calculated with different source impedance than that of the passive loading condition of all other elements. To derive such results, a rank-one update of the loaded array admittance matrix was performed. Such a practice is also applicable if one of the passive elements is terminated diversely than all the others, as well as than the source impedance of the EEP at hand. For the simple case of one failed element termintaion, we show that only one entry from each EEP set (nominal and faulty) is needed to identify the new impedance value.

As phased array systems become larger and more difficult to characterize, Unmanned Aerial Vehicle (UAV) measurements of EEPs become an appealing method of array characterisation [4]. Aperture arrays for low-frequency radio astronomy, such as the Square Kilometer Array (SKA) [5] and its precursors, could benefit from the proposed method of fault diagnosis. From a practical standpoint, this method offers an advantage of being simpler, and is applied by monitoring the EEP of only one reference element, reducing the number of required EEPs to reconstruct the load matrix. Practically, all information in extracting the antenna termination resides in the sampled points of the electric field of one selected element.

In Sec. 2, we introduce the calculation, its network equivalent and discuss possible applications in the context of UAV measurements. In Sec. 4 the resulting equation is verified on a dipole array simulation, as well as on a 4-by-4 tile of the Murchison Widefield Array (MWA).

2 EEPs with a Faulty Termination and Inverse Impedance Equation

Let us suppose that in an array of N elements, such as that of Fig. 1, element k has a faulty termination and instead of Z_L it is loaded with an impedance of $Z_F = Z_L + \Delta Z$. In this case, the most convenient source for EEP calculation is a Thevenin voltage source V_g, $Z_g = Z_L$ for each element $n \in \{1, \dots N\}$ [1]. As in [3], we use the network of Fig. 1 to first calculate the open-circuit currents $I_n^{k,oc} = (\mathbf{Z}_A + \mathbf{Z}_L^k)^{-1}\mathbf{V}_{g,n}$, where $\mathbf{V}_{g,n} = [0 \dots V_g \dots 0]$ with a non-zero entry only at the n-th position, while the load matrix in this case can be written as: $\mathbf{Z}_L^k = Z_L\mathbf{I} + (\Delta Z)\mathbf{u}_k\mathbf{u}_k^T$ where $\mathbf{u}_k = [0 \dots 1 \dots 0]$ a unit vector with an entry only at position k. Therefore $I_n^{k,oc} = [(\mathbf{Z}_A + \mathbf{Z}_L^k)^{-1}\mathbf{V}_{g,n}]_n = V_g \mathrm{col}_n\{\left(\mathbf{Z}_A + Z_L\mathbf{I} + (\Delta Z)\mathbf{u}_k\mathbf{u}_k^T\right)^{-1}\}$, where $\mathrm{col}_n\{\cdot\}$ extracts column n from its matrix argument. For brevity let us define the loaded admittance matrix $\mathbf{Y} = (\mathbf{Z}_A + Z_L\mathbf{I})^{-1}$ of the identically loaded elements, and the loaded admittance matrix $\mathbf{Y}_k = (\mathbf{Z}_A + Z_L\mathbf{I} + (\Delta Z)\mathbf{u}_k\mathbf{u}_k^T)^{-1}$ when antenna k has a faulty termination. By using the Sherman-Woodburry-Morrison formula and the symmetry property $\mathbf{Y} = \mathbf{Y}^T$, the inverse matrix in the column operation is written as:

$$\begin{aligned}\mathbf{Y}_k &= \mathbf{Y} - \frac{(\Delta Z)\mathbf{Y}\mathbf{u}_k\mathbf{u}_k^T\mathbf{Y}}{1+(\Delta Z)[\mathbf{Y}]_{kk}} \\ &= \mathbf{Y} - \frac{(\Delta Z)\mathrm{col}_k\{\mathbf{Y}\}\mathrm{col}_k\{\mathbf{Y}\}^T}{1+(\Delta Z)[\mathbf{Y}]_{kk}} \end{aligned} \tag{1}$$

Applying now the $\mathrm{col}_n\{\cdot\}$ operation we have:

$$\begin{aligned}&\mathrm{col}_n\{\mathbf{Y}_k\} = \mathrm{col}_n\{\mathbf{Y}\} - \frac{(\Delta Z)}{1+(\Delta Z)[\mathbf{Y}]_{kk}} \times \\ &\mathrm{col}_n\{\mathrm{col}_k\{\mathbf{Y}\}\mathrm{col}_k\{\mathbf{Y}\}^T\} \\ =&\mathrm{col}_n\{\mathbf{Y}\} - \lambda_k[\mathbf{Y}]_{nk}\mathrm{col}_k\{\mathbf{Y}\} \end{aligned} \tag{2}$$

where $\lambda_k = (\Delta Z)/(1+(\Delta Z)[\mathbf{Y}]_{kk})$ The n-th EEP of this formulation is expressed with respect to the oc-EEPs (referred to ideal current source I_g) as $E_n^{\mathbf{Z}_L^k} = V_g/I_g\mathrm{col}_n^T\{\mathbf{Y}_k\}\mathbf{E}^{\mathrm{oc}}$. If we stack all N such equations in a column, then we can get:

$$\begin{aligned}\mathbf{E}^{\mathbf{Z}_L^k} &= \frac{V_g}{I_g}\begin{bmatrix}\mathrm{col}_1^T\{\mathbf{Y}_k\} \\ \vdots \\ \mathrm{col}_N^T\{\mathbf{Y}_k\}\end{bmatrix}\mathbf{E}^{\mathrm{oc}} \\ &= \frac{V_g}{I_g}\left(\begin{bmatrix}\mathrm{col}_1^T\{\mathbf{Y}\} \\ \vdots \\ \mathrm{col}_N^T\{\mathbf{Y}\}\end{bmatrix} - \lambda_k\begin{bmatrix}[\mathbf{Y}]_{1k}\mathrm{col}_k^T\{\mathbf{Y}\} \\ \vdots \\ [\mathbf{Y}]_{Nk}\mathrm{col}_k^T\{\mathbf{Y}\}\end{bmatrix}\right)\mathbf{E}^{\mathrm{oc}} \\ &= \frac{V_g}{I_g}(\mathbf{Y}^T - \lambda_k\mathrm{diag}(\mathrm{col}_k\{\mathbf{Y}\})\mathrm{Col}_k^T\{\mathbf{Y}\})\mathbf{E}^{\mathrm{oc}} \end{aligned} \tag{3}$$

where $\mathrm{diag}(\cdot)$ means the diagonal matrix of the argument and $\mathrm{Col}_k\{\mathbf{Y}\}$ is a $N\times N$ matrix where $\mathrm{col}_k\{\mathbf{Y}\}$ is repeated N times. But $V_g/I_g\mathbf{Y}^T\mathbf{E}^{\mathrm{oc}} = \mathbf{E}^{\mathbf{Z}_L}$ [1] and $V_g/I_g\mathrm{Col}_k^T\{\mathbf{Y}\}\mathbf{E}^{\mathrm{oc}} = [E_k^{\mathbf{Z}_L}\ldots E_k^{\mathbf{Z}_L}]^T = E_k^{\mathbf{Z}_L}\mathbf{1}$, where $\mathbf{1} = [1\ldots 1]^T$. Finally:

$$\begin{aligned}\mathbf{E}^{\mathbf{Z}_L^k} &= \mathbf{E}^{\mathbf{Z}_L} - \lambda_k E_k^{\mathbf{Z}_L}\mathrm{diag}(\mathrm{col}_k\{\mathbf{Y}\})\mathbf{1} \\ &= \mathbf{E}^{\mathbf{Z}_L} - \lambda_k E_k^{\mathbf{Z}_L}\mathrm{col}_k\{\mathbf{Y}\} \end{aligned} \tag{4}$$

The k-th component of the new $\mathbf{Z}_L^k$-EEPs can be proven to be the same as calculated in [3]. It is also apparent that Eq. (4) can recursively be calculated for more rank-one updates representing more termination faults.

Another way to express Eq. (4) is by introducing the short-circuit currents $I_{ij}^{sc} = [\mathbf{Y}]_{ij}V_g$, which quantify the current induced in port i by excitation of a voltage source V_g on port j with all other ports short-circuited (the ports now refer to the $\mathbf{Z}_A + \mathbf{Z}_L$ multiport network). Let us now suppose that ΔZ is another impedance in series with Z_L in port k (not taken into account in those I^{sc} calculations). Then the n-th EEP of Eq. (4) is equal to:

$$\begin{aligned}E_n^{\mathbf{Z}_L^k} &= E_n^{\mathbf{Z}_L} - \frac{[\mathbf{Y}]_{kn}V_g\Delta Z}{V_g + [\mathbf{Y}]_{kk}V_g\Delta Z}E_k^{\mathbf{Z}_L} \\ &= E_n^{\mathbf{Z}_L} - \frac{I_{nk}^{sc}\Delta Z}{V_g + I_{kk}^{sc}\Delta Z}E_k^{\mathbf{Z}_L} \end{aligned} \tag{5}$$

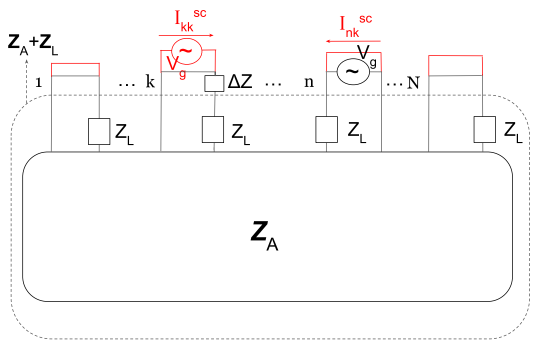

Figure 1. Network schematic of a Z_L-loaded antenna array of N elements described by its impedance matrix $\mathbf{Z}_A$, where a faulty element at position k is modelled with an extra series impedance ΔZ along the Z_L termination. The gray lines show the real excitation and termination conditions, while the red lines show the referenced ones for the voltage transfer function of the second term in Eq. (5).

The factor multiplying $E_k^{\mathbf{Z}_L}$ is the voltage transfer function from an excitation at the now unloaded port n of the $\mathbf{Z}_A + \mathbf{Z}_L$ multiport network, to what is now seen as the load in port k, which is ΔZ. This concept is also illustrated in Fig. 1, where the red schemes show the contribution of the faulty element expressed by the voltage transfer function. It is also worth mentioning the result if $n = k$. Then:

$$E_n^{\mathbf{Z}_L^k} = \frac{V_g}{V_g + I_{kk}^{sc}\Delta Z}E_k^{\mathbf{Z}_L} \tag{6}$$

In this case the circuit equivalent calculates only the contribution by the short-circuit current on the excited port itself, which in circuit theory is known as a voltage divider.

A possible application of this formula is finding Z_F from a measurement of the array $\mathbf{Z}_L^k$-EEPs (under faulty termination), when the $\mathbf{Z}_L$-EEPs and the impedance matrix $\mathbf{Z}_A$ are known. Since there is only one unknown, we can use just one component (the n-th) of Eq. (4) which leads to:

$$E_n^{\mathbf{Z}_L^k} = E_n^{\mathbf{Z}_L} - \frac{(\Delta Z)[\mathbf{Y}]_{nk}}{1+(\Delta Z)[\mathbf{Y}]_{kk}}E_k^{\mathbf{Z}_L} \Rightarrow \tag{7}$$

$$Z_F = Z_L + \frac{E_n^{\mathbf{Z}_L} - E_n^{\mathbf{Z}_L^k}}{[\mathbf{Y}]_{nk}E_k^{\mathbf{Z}_L} - [\mathbf{Y}]_{kk}(E_n^{\mathbf{Z}_L} - E_n^{\mathbf{Z}_L^k})} \tag{8}$$

This equation implies that the position k of the faulty termination is known, but that is usually not the case. In the more general case of unknown k, Eq. (8) has to be iterated for $k = 1,\ldots,N$ until it is satisfied for a certain k. Moreover, only one zenith angle measurement point is needed for this equation to work. Multiple points might nonetheless offer a more robust estimation when measurement uncertainties impact the calculations, by solving a least squares problem instead of an exact algebraic inversion of Eq. (7).

3 Dipole Array Verification

In this section, we present a verification of Eq. (4) on simulated EEPs of a 3-element triangular dipole array in the dense regime. Dipole #1 is placed in the origin of the coordinate system, dipole #2 is located on the x-axis and dipole #3 is on the y-axis. The dipoles have the same length $l = 0.5\lambda$ at $f_0 = 300$ MHz, and the dipole separation is $R_{12} = 0.12\lambda$ along the x-axis, $R_{13} = 0.1\lambda$ along the y-axis. A dense-regime array is chosen because of the stronger mutual coupling, which is expected to be seen in EEPs. Furthermore, dipole #2 on the x-axis has a load of $Z_F = 10\ \Omega$, while the other two are terminated with nominal $Z_L = 50\ \Omega$. Fig. 2 shows the co-polar ($\hat{\theta}$) and cross-polar ($\hat{\phi}$) EEPs for all 3 dipoles across zenith angle in E-plane. The simulated ("sim.") curves are FEKO simulations, while the calculated ("calc.") curves result from the application of Eq. (4) for $n = 1,2,3$ with simulated EEPs of the nominal configuration when all elements are terminated with $Z_L = 50\ \Omega$. Perfect agreement of the simulated and calculated patterns for both co-polar and cross-polar components confirms the validity of the derived formula. It can be seen that the dipole terminated with a faulty load ($n = 2$) has a more pronounced pattern, in accordance with the stronger influence of the self-induced short-circuit current I_{22}^{sc} with respect to the inter-element ones I_{12}^{sc}, I_{32}^{sc}.
We now proceed to demonstrate how the knowledge of one EEP from each of the two sets (nominally loaded and single-fault cases) can recover the impedance fault Z_F using Eq. (8). On the examined dipole array, we assume the knowledge of co-polar patterns $E_{1,\theta}^{\mathbf{Z}_L}$, $E_{1,\theta}^{\mathbf{Z}_L^2}$ at a 1° zenith angle sampling over the E-plane cut ($\phi = 0^\circ$). As per our previous notation and the dipole numbering, '1' in the subscript means that we know the Dipole #1 EEPs, while $\mathbf{Z}_L^2$ on the superscript of the second EEP means that Dipole #2 has a faulty load. It will be assumed though that the faulty dipole position is not known, such that our second EEP can be for this exercise named $E_1^{\mathbf{Z}_L'}$. To find both k and Z_F, we iterate Eq. (8) 3 times, replacing $k = 1,2,3$ in $[\mathbf{Y}]_{1k}$, $[\mathbf{Y}]_{kk}$ for every θ in $[0^\circ,\ 180^\circ]$. Fig. 2c shows the real and imaginary parts of Z_F for all 3 cases across θ. The only case that returns constant values for all tested points is $k = 2$, since the green curves are almost perfectly horizontal lines. This confirms that $k = 2$ is the correct number for the faulty dipole. The Root-Mean-Square (RMS) error across θ of the complex Z_F with respect to the true, $10\ \Omega$ value is 7.5 mΩ, thus confirming the high numerical accuracy in extracting the impedance fault with Eq. (8).

4 MWA Tile Verification

In another example, we demonstrate that Eq. (8) can also be verified using a tile of the MWA. This is a planar regular 4-by-4 array of 16 wideband bow-tie antennas whose performance has extensively been characterised [6]. Fig. 3a shows an MWA tile mounted on a rectangular metal grid acting as a ground plane located in the Murchison Radio Astronomy Observatory (MRO). MWA operates in the 70-300 MHz band and has a 30 deg^2 field of view, enabling of observations of various scientific interests, including solar, heliospheric and ionospheric studies. Due to the harsh environmental conditions in the Australian outback, some LNAs have been found to malfunction after long periods of operation, thus rendering the respective antennas dormant. While such outages are predicted by the complete degeneration of the digitiser voltage outputs, milder deviations of the input impedance can only be predicted by more sophisticated diagnostic measurements. In what follows, we will use FEKO EEP simulations, neglecting random noise occuring in UAV measurements or other systematics.
Two sets of EEPs have been simulated for the MWA tile:

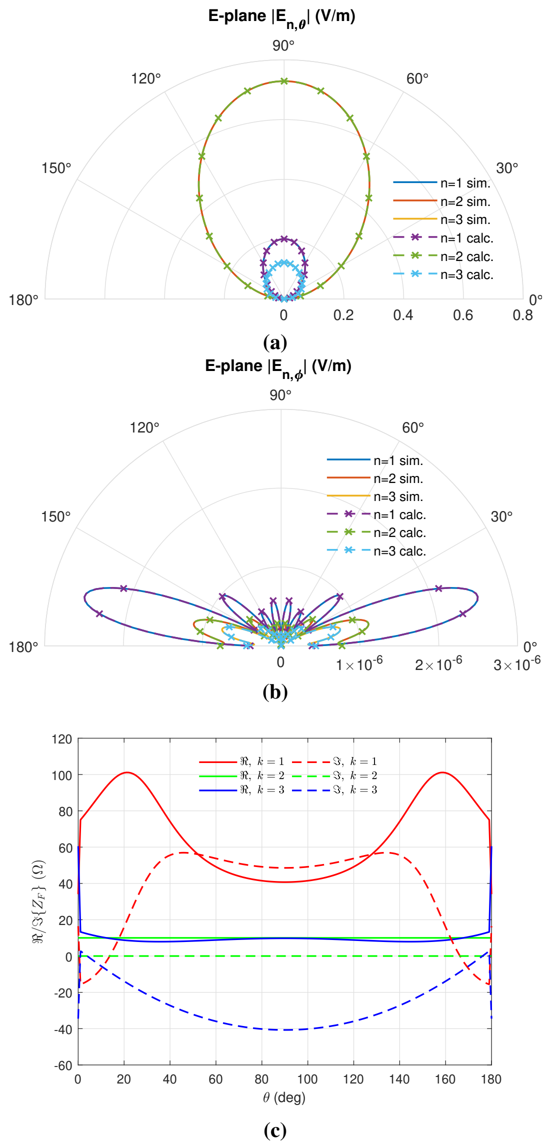

Figure 2. (a) $\hat{\theta}$-component (co-polar) and (b) $\hat{\phi}$-component (cross-polar) of all the 3 EEPs of a dipole configuration, directly simulated by FEKO and calculated using Eq. (4) and the simulated EEPs under nominal ($50\ \Omega$) termination. (c): $\Re\{Z_F\}$ and $\Im\{Z_F\}$ in Ω, applying Eq. (8) for $k = 1,2,3$ across zenith angles of the E-plane of the $E_{1,\theta}^{\mathbf{Z}_L}$, $E_{1,\theta}^{\mathbf{Z}_L'}$ EEPs.

one with its nominal LNA load $Z_{LNA} = 887.3 + j155.3\ \Omega$ [2] on all antennas, and another set of EEPs with a faulty element with $Z_F = 28.74 + j15.98$ [2], both at 128 MHz. Fig. 3b shows the RMS errors calculated using Eq. (8) assuming knowledge of the patterns $E_n^{\mathbf{Z}_L}$, $E_n^{\mathbf{Z}'_L}$ on the E-plane. The RMS operates over all θ angles, while the legend shows all n possible antennas. We set an upper limit of $|Z_F| \cdot 10\%$ and discard all higher RMS errors in the plot. It can be seen that whichever n-th EEP we use, $k = 1$ is always found (in red) as the RMS minimum coinciding with the true faulty antenna number, with errors of the order of 10^{-13}. Furthermore, the 1st element along with its closest neighbors ($n = 2$ and $n = 5$) present RMS values within our chosen threshold, while for the 13-th element, all EEPs show astonishingly low RMS errors when position $k = 13$ is assumed as that of the faulty element. These observations are expected to be useful in subsequent analysis with noisy EEPs, where minimization of the RMS error is not guaranteed to always lead in the correct element position.

(a)

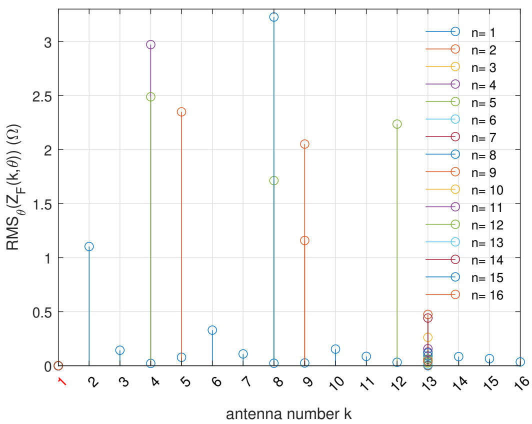

(b)

Figure 3. (a): An MWA tile mounted on a rectangular ground plane at MRO. (photo credit: M. Kovaleva), (b): RMS over all θ angles of complex Z_F (Ω) calculated with Eq. (8) using all possible antennas. The minimum (in red) indicates the position of the faulty antenna, while the legend shows all possible antenna cases for the choice of EEPs.

5 Conclusion

In this summary paper, utilisation of rank-one update linear algebra techniques has been employed to derive the EEPs of an array when a certain element presents a termination fault. The resulting equation can easily be inverted to compute the new impedance value when two EEPs, one under each loading condition, are assumed to be known. Application of both the forward and inverse, impedance calculation is found both on a simple 3-dipole array, as well as in a MWA 16-element tile, with a high level of accuracy with respect to the simulated EEPs or true impedance faults initially set in such simulations.

Acknowledgment

We acknowledge the Wajarri-Yamatji people as the traditional owners of the Inyarrimanha Ilgari Bundara (Murchison Radio-astronomy Observatory) site.

References

[1] K. F. Warnick, D. B. Davidson and D. Buck, “Embedded Element Pattern Loading Condition Transformations for Phased Array Modeling," in *IEEE Transactions on Antennas and Propagation*, vol. 69, no. 3, pp. 1769-1774, March 2021, doi: 10.1109/TAP.2020.3027593.

[2] M. Kovaleva, D. Ung, A. Sutinjo, B. Juswardy, D. B. Davidson and R. B. Wayth, “Analysis of the Loading Effect of Faulty LNAs on Embedded Element Patterns in the Murchison Widefield Array," in *14th European Conference on Antennas and Propagation (EuCAP)*, Copenhagen, Denmark, 2020, pp. 1-4, doi: 10.23919/EuCAP48036.2020.9135727.

[3] D. Buck, K. F. Warnick, R. Maaskant, D. B. Davidson and D. F. Kelley, “Measuring Array Mutual Impedances Using Embedded Element Patterns," in *IEEE Transactions on Antennas and Propagation*, vol. 71, no. 1, pp. 606-611, 2023

[4] F. Paonessa, L. Ciorba, G. Virone, P. Bolli, A. Magro, A. McPhail, D. Minchin and R. Bhushan, “SKA-Low Prototypes Deployed in Australia: Synoptic of the UAV-Based Experimental Results" in *URSI Radio Science Letters*, **2**, Aug. 2020

[5] P. E. Dewdney, P. J. Hall, R. T. Schilizzi and T. J. L. W. Lazio, "The Square Kilometre Array," in *Proceedings of the IEEE*, vol. 97, no. 8, pp. 1482-1496, Aug. 2009, doi: 10.1109/JPROC.2009.2021005

[6] A. Sutinjo, J. O’Sullivan, E. Lenc, R. B. Wayth, S. Padhi, P. Hall and S. T. Tingay, “Understanding instrumental Stokes leakage in Murchison Widefield Array polarimetry”, in *Radio Science*, vol. 50, no. 1, pp. 52-65, 2015, doi: 10.1002/2014RS005517